668–674 Nucleic Acids Research, 1997, Vol. 25, No. 3

Altered structure of the DNA duplex recognized by yeast transcription factor Reb1p

Darrell R. Davis* and David J. Stillman[1]

Department of Medicinal Chemistry and [1]Division of Molecular Biology and Genetics, Department of Oncological Sciences, University of Utah, Salt Lake City, UT 84112, USA

Received July 30, 1996; Revised and Accepted November 22, 1996

ABSTRACT

The *Saccharomyces cerevisiae REB1* gene encodes a sequence-specific DNA binding protein that has been implicated in chromatin structure, transcription regulation and transcription termination. Previous work has shown that the DNA sequence recognized by Reb1p contains an adenosine residue that is unusually reactive toward chemical modification by dimethylsulfate and that methylation of this nucleoside increases the binding affinity of the Reb1p protein for its target. Prompted by these results, we determined the solution structure of the 13mer Reb1p DNA duplex recognition site d(GTCCGGGTAATGC)·d(GCATTACCCGGAC) using 2D NMR, distance geometry and iterative 2D NOESY back-calculation structure refinement. The distance geometry-refined molecule demonstrated an unusual structure in the TAAT region of the sequence that was manifested in cross-strand base stacking, as indicated by unusually strong NOE interactions between H2 protons on three adjacent adenosine bases. This structure was compared to two published NMR studies of DNA duplexes containing the related sequence TAAC. The Reb1p DNA structure does not show the conformational mobility or the 'transient kink' at TpA steps characteristic of the related TAAT-containing sequences.

INTRODUCTION

The *Saccharomyces cerevisiae REB1* gene encodes an abundant 125 kDa DNA binding protein that shows homology to the Myb DNA binding protein (1,2). Disruption of *REB1* is lethal and thus *REB1* is an essential gene. The Reb1p DNA binding protein was first identified as binding to sites within the enhancer/terminator region of the tandemly repeated rRNA genes of *S.cerevisiae* (3). More recently it has been shown that the Reb1p binding site is an essential component of the RNA polymerase I transcription terminator (4,5). Reb1p binding sites have also been identified in a number of promoters of genes transcribed by RNA polymerase II and thus Reb1p has been implicated in transcription regulation (6–13). Depending upon the exact context, a Reb1p binding site can either enhance or inhibit transcription activation by transcription factors bound nearby and thus the exact context strongly affects Reb1p activity *in vivo* (8,10,13). It has been suggested that Reb1p affects RNA polymerase II transcription by affecting chromatin structure, as the Reb1p binding site has been shown to create a 230 bp nucleosome-free region at the *GAL1-10* promoter *in vivo* (14).

In the course of identifying the DNA target sequence for the Reb1p protein, we observed that one of the A residues within the duplex was reactive to dimethylsulfate, contrary to the expectation for double-stranded DNA (13). The methylated DNA was then observed to bind tighter to Reb1p protein than the unmethylated sequence, suggesting that an altered structure could be important for protein–DNA recognition. We have determined the solution structure of the non-self-complementary Reb1p DNA 13mer duplex d(GTCCGGGTAATGC)·d(GCATTACCCGGAC) using distance geometry and 2D NOESY back-calculation refinement. The Reb1p DNA structure containing the TAAT sequence is compared with two published structures of DNA duplex structures containing the TAAC sequence. One structure is the recognition site for the Myb oncogenic protein (15) and the other DNA sequence is a high affinity binding site for the drug (+)-CC-1065 (16).

MATERIALS AND METHODS

Sample preparation

The two DNA strands (5′-GTCCGGGTAATGC-3′ and 5′-GCATTACCCGGAC-3′) corresponding to the Box2 Reb1p binding site from the *SIN3* promoter (13) were synthesized on an Applied Biosystems 380 DNA synthesizer using solid-phase phosphoramidite chemistry. The DNA was deprotected by treatment with 3:1 ammonia:ethanol for 12 h at 55°C, then purified by gel filtration chromatography on Superfine Sephadex G-25. The complementary strands were dissolved in 0.5 ml 100 mM NaCl and then combined in equimolar amounts based on A_{260} UV measurements. The DNA duplex was annealed by heating to 90°C and cooling to 25°C over 4 h. The double-stranded DNA was separated from single strands by hydroxyapatite chromatography using a phosphate gradient as described by Kintanar *et al.* (17), then the DNA duplex was desalted on a Sephadex G-10 column. The purified, desalted DNA duplex was lyophilized and redissolved in 0.5 ml 25 mM phosphate buffer, pH 7.0, containing 25 mM sodium chloride and 0.2 mM EDTA to give a final concentration of 5 mM. The sample was twice lyophilized from 99.96% D_2O (Cambridge Isotopes), dissolved in 0.5 ml 99.996% D_2O and transferred to a 5 mm NMR tube.

*To whom correspondence should be addressed. Tel: +1 801 581 7006; Fax: +1 801 581 7087; Email: davis@adenosine.pharm.utah.edu

NMR spectroscopy

All NMR experiments were done using a Varian Unity 500 MHz NMR spectrometer and a Nalorac ID500 indirect detection probe. 2D NOESY, TOCSY, TOCSY-NOESY, ROESY and PECOSY experiments were collected as hypercomplex data sets using TPPI-States phase cycling (18) and processed with VNMR (Varian) and FELIX (Biosym) software. The F_2 data were collected with 4096 total data points and 400 t_1 increments were zero-filled to 2048 total points in F_1. The time domain NOESY (19) data were weighted with a skewed, 90° phase-shifted sine bell with length equal to the number of data points. The first data points in F_1 were corrected by multiplying by a constant equal to 0.5 (20). NOESY spectra were collected with the mixing time randomly varied by 10% to suppress zero-quantum contributions to cross-peaks between scalar-coupled spins at short mixing times (21). TOCSY experiments were collected in the clean mode with a MLEV-17 mixing sequence (22,23). The TOCSY-NOESY experiments were performed as previously described (24,25). The ROESY (26,27) experiments were collected using a time-shared spinlock field of ~3500 Hz. PECOSY (28) spectra were collected with WALTZ-16 ^{31}P decoupling and a decoupler field strength of ~500 Hz to minimize sample heating.

Distance measurements

Preliminary distance estimates were calculated from 2D NOE build-up rates using the two-spin approximation at short mixing times (29). The integrated 2D volumes were used to generate cross-peak intensity build-up plots that were converted into distances by scaling the initial rates against the build-up rates for cytosine H5–H6 NOEs corresponding to a known distance of 2.46 Å. A single correlation time was assumed for the entire molecule with the exception of distances involving methyl groups, which were referenced to a thymidine H6–methyl distance of 2.9 Å. The assumption of a single correlation time is convenient for initial distance estimates and was validated in this study by the accurate back-calculation of all NOESY cross-peaks involving fixed distances, including the H5–H6 and H2′–H2″ cross-peaks corresponding to known fixed distances on the bases and sugars respectively.

Distance geometry structure refinement

Distance geometry-based structure refinement was done on a Silicon Graphics Indigo2 workstation using DSPACE 5.0 (Biosym). The basic principles of distance geometry have been previously described (30,31) as well as how these principles are implemented within the context of the DSPACE program (32–34). Simulated annealing was performed in the 'random' mode, which does not use SHAKE to maintain bond lengths and angles; the trajectories were regulated with Brownian damping set to 0.02, a spring factor of 0.005 and a sensitivity of 0.01. Structures were refined from B-form coordinates using six repetitions of the random annealing cycle. Each cycle consisted of 128 increments which were iterated eight times. Structures refined from either A-form coordinates of random embedded starting structures were superimposable on structures refined from B-form coordinates, but typically required at least 20 repetitions of the annealing protocol for convergence.

NOE back-calculation

NOESY spectra were calculated from the DSPACE refined structures using the program BKCALC (Hare Research). BKCALC simulates the NOESY spectrum by numerical integration of the Bloch equations for a relaxation network defined by the coordinates of a molecular structure (34). The cross-relaxation and leakage rate parameters in the simulation were determined experimentally and resulted in an extremely accurate reproduction of the diagonal decay rates for all protons, as well as the build-up rates for the cytidine H5–H6 cross-peaks and the sugar H2′–H2″ cross-peaks corresponding to known fixed distances. The leakage rate was determined directly from the experimental NOESY spectra by adding up all of the rows within a spectrum to obtain a 1D projection. The projected spectra as a function of mixing time are fitted to an exponential decay curve to determine the leakage parameter, since the cross-relaxation is accounted for in the projections. The cross-relaxation parameter is then the only remaining variable to the relaxation calculation and was determined by iterative simulation of the H5–H6 experimental build-up curves. An interproton cut-off distance of 5 Å and a time increment of 1 ms was used for all the BKCALC simulations.

RESULTS

NMR assignment and constraint determination

Sequential assignment of the 2D NOESY spectrum is a necessary prerequisite for distance constraint measurement. The well-established sequential NOE assignment strategy (35–37) was supplemented with 2D TOCSY-NOESY experiments (24,25). The TOCSY-NOESY experiment was essential for assigning the consecutive GC base pairs. During the TOCSY period of the TOCSY-NOESY, magnetization is transferred from the H5 to H6 scalar-coupled protons. The subsequent NOE period transfers magnetization to protons that normally give NOEs with the H6 protons, such as sugar H1′ and H2′,H2″ protons. For the assignment of the Reb1p spectrum, the most useful additional resonances were from the cytosine H5 protons to the sugar H1′ protons of the same residue. A comparison of Figure 1a and b shows how this additional information was used. In the NOESY spectrum of Figure 1a, no cross-peaks are observed between the H5 protons and sugar H1′ on the same residue. In the TOCSY-NOESY spectrum in Figure 1b, cross-peaks are seen between the cytosine H5 protons and both the (n – 1) H1′ protons and the intraresidue H1′ protons. The only situation where these sequential connectivities are not seen is for C_4 and C_{22}, where the H5 and H1′ protons have nearly coincident chemical shifts.

Once the H5 assignments were made with assistance from the TOCSY-NOESY, the remaining sequential assignments were made from the NOESY and TOCSY spectra. Figure 2 shows the base–H1′ and base–H2′,H2″ region of the NOESY spectrum. 2D NOESY spectra were collected at mixing times of 30, 60, 90, 120 and 200 ms. Cross-peak volumes were measured for all resolved cross-peaks and used to generate individual build-up rate plots for NOE cross-relaxation. Approximately 279 experimental interproton distances were measured from NOE cross-peak volumes. These experimental NOE restraints were supplemented with hydrogen bond restraints inferred from imino spectra in H_2O, lower bound restraints for aromatic–H5′,H5″ protons as indicated by the lack of NOE cross-peaks and a limited number of torsion angle restraints for α, γ and ε determined by limits on ^{3}J scalar couplings

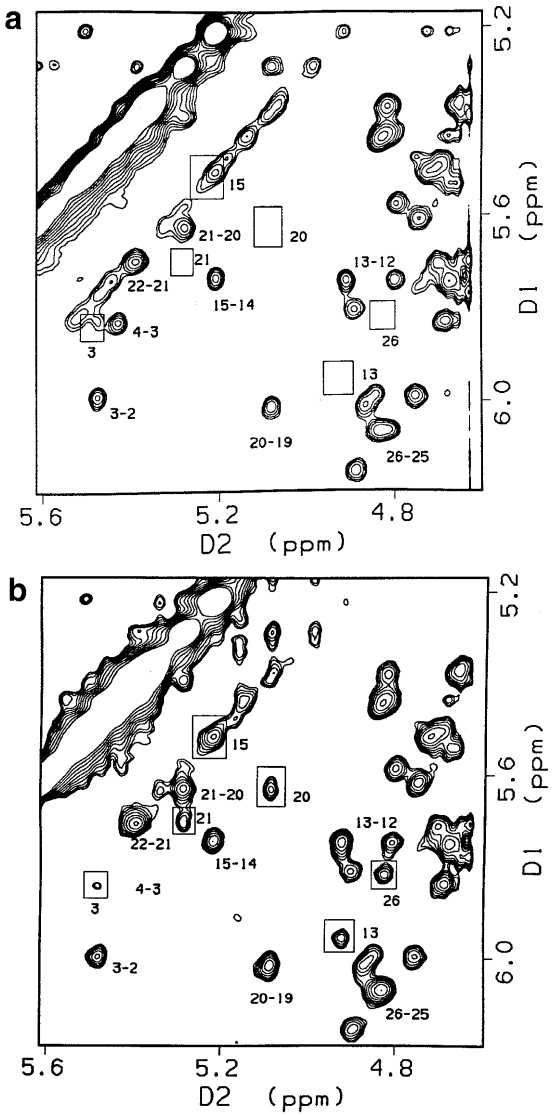

Figure 1. (**a**) An expansion showing the cytosine H5–sugar H1′ cross-peaks in the 120 ms NOESY spectrum. The small boxes indicate the position of the intranucleotide cross-peaks seen in (b). The numbered peaks not in the boxes are the interresidue H5–H1′ peaks. (**b**) Expansion of the TOCSY-NOESY spectrum. Intraresidue, TOCSY relayed NOE cross-peaks are boxed and numbered.

determined from PECOSY cross-peaks and NOESY lower bound constraints as described by Reid and co-workers (38). The combination of restraints was used to generate a distance matrix for refining the structure.

Distance geometry and back-calculation refinement

Starting structures were generated by embedding the distance matrix containing the experimental constraints into 3-space or by starting from idealized A- or B-form coordinates. A regimen combining conjugate gradient refinement and simulated annealing was used to generate a family of structures. A representative structure was chosen for back-calculation refinement and the NOESY spectrum calculated at each of the experimental mixing times. The calculated spectra were visually inspected and cross-peaks that differed in the experimental and calculated data were analyzed to determine the nature of the disagreement. Interproton distances were measured in the structure and compared with the restraint file to determine whether the offending cross-peak represented an NOE violation or if the proton pair was unconstrained. The appropriate action was then taken to either alter the distance restraint or add a restraint and the structure then submitted to another round of refinement. After several rounds of iterative back-calculation refinement, the structure was refined beginning anew from a B-form starting structure. This process of comparing the experimental and calculated NOESY spectra, altering the bounds matrix, followed by additional refinement was repeated until the calculated spectra and the experimental spectra matched, as shown in Figure 3. During the iterative refinement process, narrow distance bounds (±0.1–0.3 Å) were only used for cross-peaks clearly visible in either the 30 or 60 ms NOESY data, while cross-peaks building up at later mixing times were allowed to float, with relaxed ±0.5 Å distance bounds.

A specific example of this approach was the inclusion of restraints for the aromatic–H3′ cross-peaks, which get most of their intensity via an indirect pathway involving aromatic to H2′,H2″ followed by H2′,H2″ to H3′ cross-relaxation. We found that although there was a large range of intensities in the aromatic–H3′ NOEs, these cross-peaks could be simulated indirectly by accurate simulation of both the aromatic–H2′,H2″ and H2′,H2″–H3″ cross-peaks. Back-calculation also allowed us to determine additional constraints from cross-peaks in poorly resolved regions. Partially overlapping peaks in the original data that could not be individually integrated accurately could be visually compared with calculated spectra. Distances within the structure were then measured to determine likely candidates that might contribute to an overlapped calculated cross-peak that did not match the intensity of the same cross-peak in the experimental spectrum. In this way it was possible to make educated guesses about the interproton distance in error and subsequently correct the restraint. Due to the excellent chemical shift dispersion for a non-self-complementary sequence this large, we did not have to resort to empirical correction in many instances; only a few restraints in the crowded base–H2′,H2″ region were corrected in this manner.

Distance geometry combined with iterative back-calculation refinement resulted in a DNA structure that matched the experimental data quite well. Figure 4 shows the superimposition of six independent structures refined from B-form coordinates. The pairwise RMSDs for the structures were in the range 0.4–0.7 Å. Superimpositions of structures refined from embedded starting structures were in the range 1.5–2.0 Å for all atoms and 0.4–0.7 Å for either the first 6 or last 7 bp. The superimpositions for the last 7 residues were always better than the first 6 bp due to the extensive constraint network in the minor groove for the A+T-rich region. The average of the NOE violations over the six structures was <0.3 Å for any particular NOE distance constraint and the DSPACE sums-of-squares penalty function was <5 $Å^2$ for each structure.

Structure analysis

The NOESY spectrum contains many structural features that indicate Reb1p is not a regular B-form structure. Most striking are the strong NOEs between the H2 protons of A9 and the H2[10] and H2[19] protons (Fig. 2c). These NOEs were so anomalous and intense for cross-peaks in the aromatic–aromatic region that we were initially concerned that they might be due to chemical

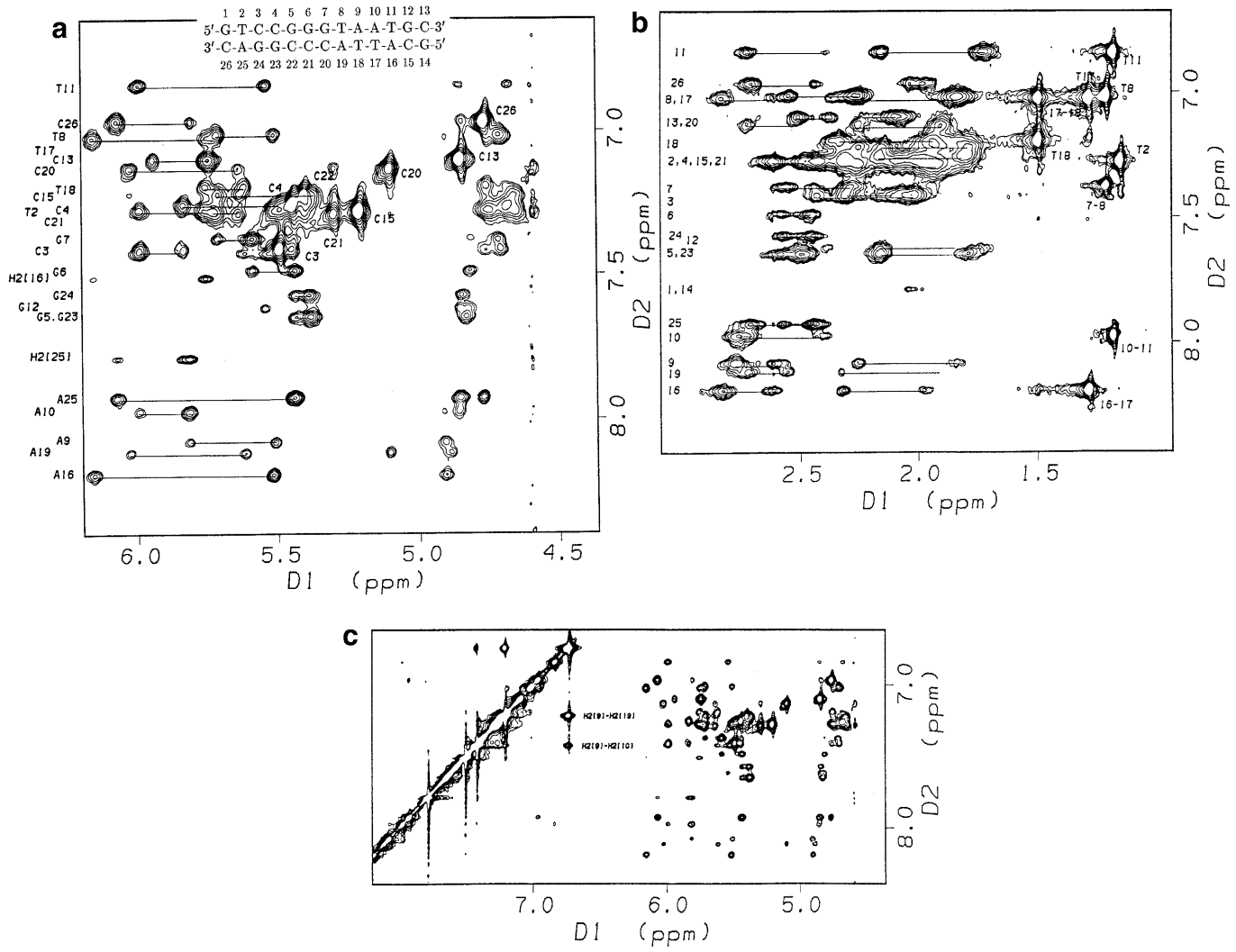

Figure 2. Expansions of the 120 ms 2D NOESY spectrum. (**a**) Base–H1′,3′,4′,5′,5″ region, (**b**) base–H2′,2″ region and (**c**) expansion showing the anomalous H2–H2 NOEs as well as the base–H1 region for comparison of cross-peak intensities.

exchange. A ROESY experiment (data not shown) confirmed that the cross-peaks are due to NOE cross-relaxation, since the H2–H2 peaks have the same sign as the other NOEs and have opposite sign compared with the diagonal. These NOEs correspond to interproton distances of 3.4 and 2.9 Å for the H2[9]–H2[10] and H2[9]–H2[19] pairs respectively. The effect of these distance constraints on the structure is to underwind the molecule at the 9–10 step to improve A–A stacking and also to force the helix axis to slide out at the 8–9 step. In the base–H1′ region shown in Figure 2, there are marked intensity differences for the H8[10]–H1′[10] and H8[10]–H1′[9] cross-peak pairs and also for the corresponding peaks involving H6[17], the base pair partner of A10. The intra- and interresidue base–H1′ cross-peaks in a B-form structure are nearly the same intensity. The stronger interresidue NOEs indicate that the base has moved closer to the sugar of the $n-1$ residue. There is another set of cross-peaks for this region of the molecule that are notably absent, i.e. H2[9]–H1′ NOEs. No peaks are seen from H2[9] to either the H1′ proton of A10 or A19, while other H2[A] protons in the molecule do show typical NOEs to H1′ protons. During the back-calculation refinement, a lower bound constraint of 4.2 Å was used to keep these protons apart, since early rounds of back-calculation refinement resulted in structures giving calculated cross-peaks that were not observed experimentally. A combination of sequence and unusual local geometry in this area also affects the chemical shift of the T18 methyl, shifting it downfield relative to the other four methyls. Inspection of the final structures shows that T18 is partially stacked under T17, where it would be deshielded relative to the other T residues, which all have 5′ purine neighbors with strong ring currents placed above the thymine methyls.

As would expected from the strong H2–H2 NOEs, the stacking geometry around A9 is quite unusual. The bases for A9, A10 and A19 are stacked with the helix axis slightly displaced to accommodate the improved stacking of A19 onto A9 across the strand, as shown in Figure 5. The minor groove is opened up in this region compared to B-form, in contrast to what would normally be expected for an A+T-rich region. The opening of the minor groove would allow access to N3[A19] by dimethylsulfate, consistent with the reactivity observed by Wang *et al.* (13).

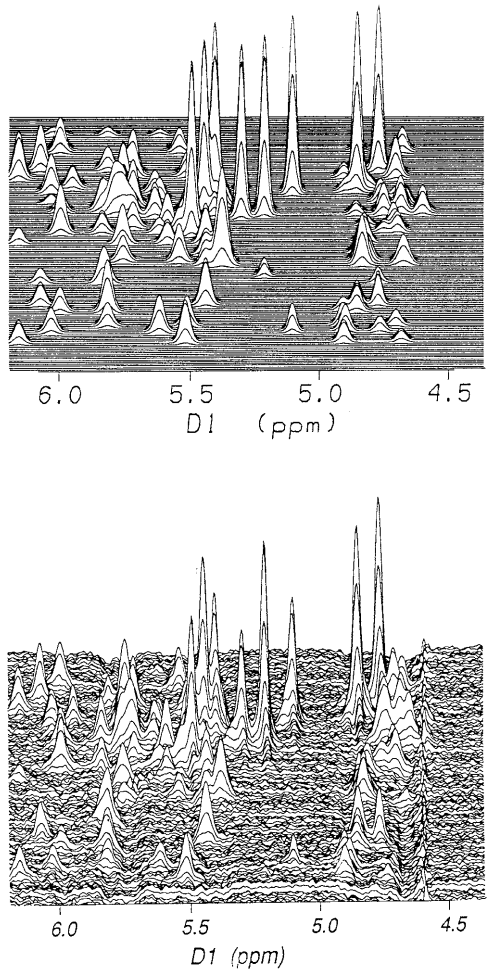

Figure 3. Back-calculation NOESY comparison of the base–H1′ region at 120 ms.

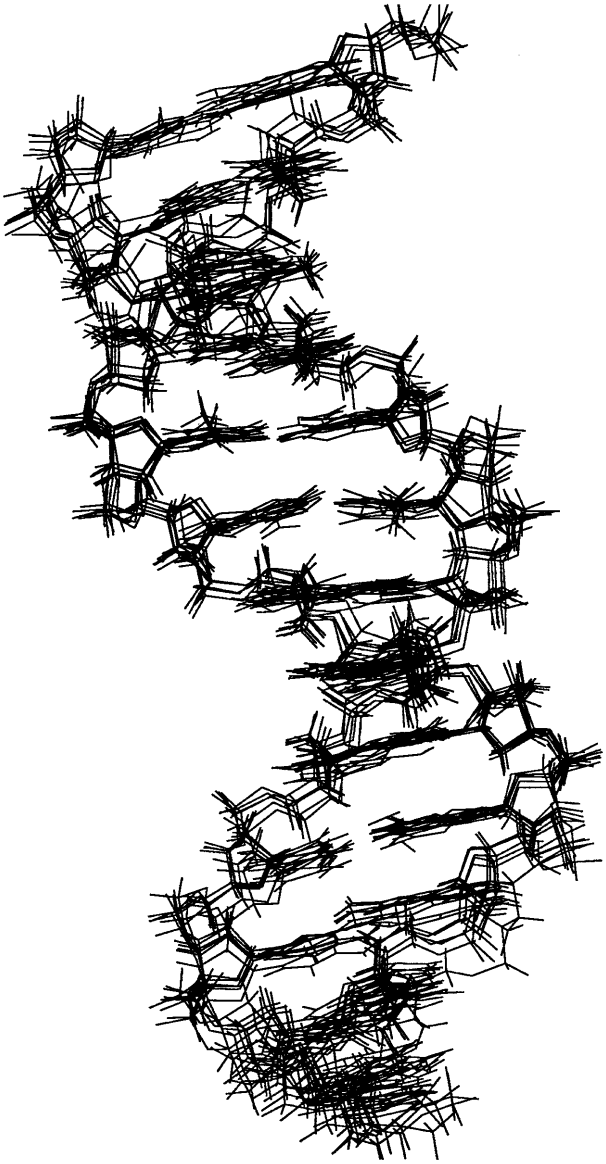

Figure 4. Superimpositions of six structures refined independently starting from B-form coordinates. The pairwise RMSDs are 0.5–0.6 Å^2.

The final, refined structure was analyzed using the NEWHELIX92 program (kindly provided by R.E.Dickerson). The pseudorotation angles are between 141 and 177°, with a mean value of 153°. The torsional angles are typical for B-form structures and the constrained α, γ and ε values are all within the set ranges. The NEWHELIX results for the structurally informative parameters, such as propeller twist, slide and buckle, are nearly B-form except within the A+T-rich region. Base pair 8–19 is buckled, as is 10–17, but in the opposite direction. Base pairs 10–17 and 11–16 are significantly propeller twisted. The average helical twist is 36.89°, with no single base step being significantly over- or underwound. The parameterization indicates that the structure is very close to B-form, even though there are significant perturbations within the A+T-rich region.

DISCUSSION

We have used 2D NMR, distance geometry and iterative 2D NOESY back-calculation structure refinement to determine the structure of a 13 bp segment of double-stranded DNA (GTCCGGGTAATGC and complement) that contains a binding site for the yeast Reb1p transcription factor. The DNA structure is anomalous in the TAAT region, as the helical axis is displaced to accommodate the stacking of the two adenosine residues. In this region the DNA is underwound, the minor groove is opened up and specific base pairs are buckled or propeller twisted.

Liaw and Brandl (39) performed binding site selection from random sequence oligonucleotides to analyze Reb1p binding. They identified a consensus sequence of CGGGTAAc for the Reb1p binding site. The lower case ‘c’ at nucleotide 8 reflects the poorer conservation at this position, with 14 out of 28 sequence binding sites containing a C; six out of 14 contain a T residue at this position, like the CGGGTAAT in our sequence.

Comparison with similar sequences

Structures have been published for two DNA sequences that are similar to the Reb1p DNA sequence. The recognition site for the Myb protein (15) and a preferential recognition sequence for (+)-CC-1065 (16) both contain the sequence TAAC, similar to the

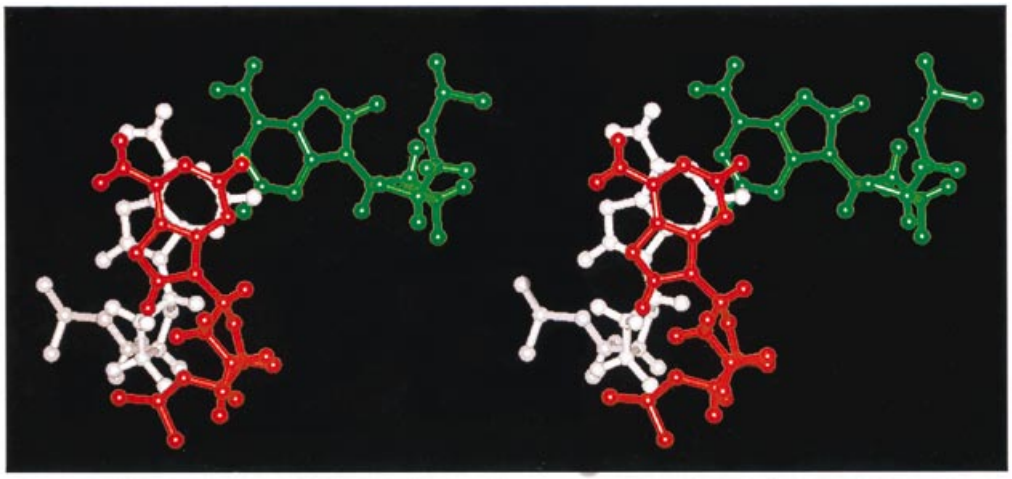

Figure 5. Adenosine residues 9 (white), 10 (red) and 19 (green) showing the stacking arrangement and the displacement of A19 toward the center of the helical axis, a position dictated by the strong H2–H2 NOEs between A9 and A19.

TAAT sequence within the Reb1p DNA site. Our sequence TAAT conforms to the consensus sequence derived for (+)-CC-1065 binding and thus we predict that our DNA would be reactive toward the drug molecule and might be expected to have a similar structure.

The Hurley sequence displays some marked similarities and also some differences with our structure. The most striking similarity is the strong H2–H2 cross-peaks for the first A (A9 in our molecule) to H2 of the following adenosine and also its cross-strand/3′ neighbor; H2[9]–H2[10] and H2[9]–H2[19]. This pattern of NOEs is also seen in the TAAC sequence of Hurley, with NOEs between H2 of the first A to the second A and the A that would be the base pair partner for the first T. Despite this similar pattern for the H2 NOEs, there are also some distinct differences in the cross-peak patterns for the well-resolved base–H1′ NOE regions of the two molecules. We see dramatic differences in the base–H1′ NOE intensities for the direct versus sequential connectivities of T17 and A10 and small differences for T8 and A9. The Hurley molecule has a pattern that deviates from B-form for the nucleotides that would correspond to base pair T11–A16 in our sequence. In contrast we observe the more extreme perturbation for A10–T17, while the relative intensities of the intra- versus interresidue base–H1′ cross-peaks for T11–A16 are almost equal. It seems that the 'transient kink' proposed by Hurley is moved 1 bp in the 5′ direction in the Reb1p sequence. Our current understanding of sequence-dependent DNA structure is clearly too primitive to provide a causal explanation for the differences observed for these closely related DNA sequences.

The Myb DNA structure is a self-complementary dodecamer and contains the same TAAC sequence as the Hurley structure. Although quantitative structural analysis of the Myb sequence has been quite extensive, there is little discussion of the qualitative NMR features that are reflected in the refined structure. In Figure S-3 of Radha *et al.* (15), it is clear that there is an NOE pattern similar to that seen by Hurley for the C residue, but the corresponding G_4 cross-peaks are of nearly equal intensity for both the intra- and interresidue base–H1′ NOEs. The differences between the two TAAC-containing molecules are much smaller than the difference between both of these and our TAAT-containing sequence.

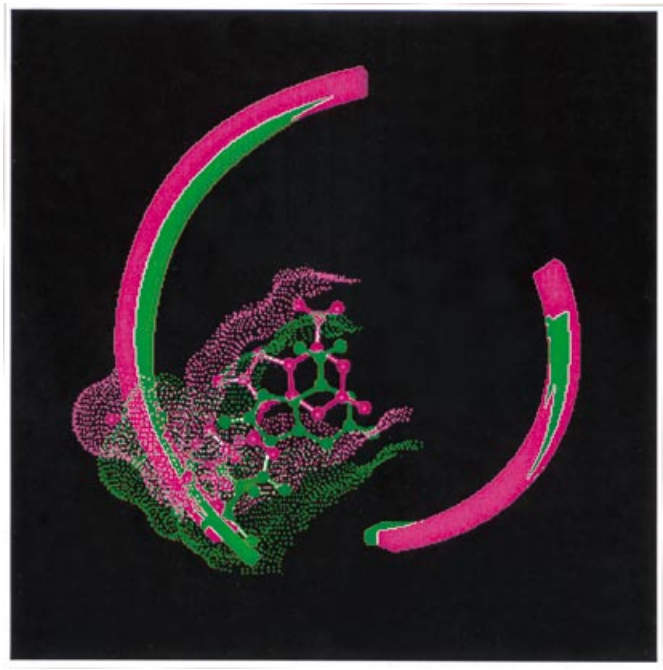

Figure 6. Superimposition of the final refined Reb1p structure (green) onto B-form coordinates (purple) in the region of the A19 residue with a ribbon through the backbone. The base for the Reb1p structure in green is displaced toward the minor groove at the bottom, allowing it to be more solvent exposed, as indicated by the Connolly surface. In contrast, the A19 residue in B-form DNA would be displaced more toward the center of the double helix.

Correlation of structure with biological function

Our studies on the structure of the Reb1p binding site were prompted by unusual results in methylation interference studies using this sequence and Reb1p protein (13). The A19 residue was observed to be unusually reactive to dimethylsulfate, indicating a structure that allowed the reagent minor groove access to this adenosine; furthermore, rather than inhibiting binding of the Reb1p protein, the methylated DNA bound the protein more

tightly. This suggested that there was an opened conformation of the DNA that was recognized by the protein and that this open conformation might be further stabilized by methylation. Figure 6 shows a comparison of the solvent accessibility for A19 in our structure and the accessibility in ideal B-form DNA. The solution structure presented here shows that the local DNA structure is anomalous around A19 and that the minor groove is opened, especially compared with a typical A+T-rich region, which would be expected to have a narrower minor groove than B-form DNA. The wider minor groove could be an important feature of protein recognition if Reb1p binds in the minor groove of its target sequence. Although we do not have evidence that this is the case, the fact that methylation improves protein binding affinity suggests that the unusual structure in the TAAT region, including the widened minor groove intrinsic to the DNA structure, could be stabilized by methylation.

The consensus sequence CGGGTAAc identified for Reb1p binding (39) differs slightly from our sequence, CGGGTAAT. Significantly, when CGGGTAAC was used in methylation interference experiments, residue A19 was not methylated (13), although Reb1p still binds. This suggests that CGGGTAAC does not contain the specific structure that leads to A19 methylation and raises the question of whether a specifically altered DNA structure is important for DNA binding by Reb1p. We note that the CGGGTAAC sequence does contain the TAAC element bound by (+)-CC-1065 and thus shows a local conformational flexibility. Thus, CGGGTAAT and CGGGTAAC, both bound by Reb1p, each have an altered DNA structure, with the 'transient kink' occurring at adjacent positions. Our structure also differs from the Hurley structure in that we see no evidence for conformational mobility at TpA steps. Lin *et al.* (16) documented the line broadening for their A16 and this general property has been extensively characterized by Reid and co-workers (40). Neither the H2 nor H8 protons of A9 in the Reb1p DNA duplex are motionally broadened. The possibility that a DNA kink and widened minor groove are essential components of DNA recognition by Reb1p await structural characterization of Reb1p–DNA complexes.

Genetic experiments indicate that the Reb1p binding site plays an important role in gene regulation. Our results showing that the Reb1p binding site has an abnormal structure raises a new question: Are the biological effects that have been ascribed to Reb1p due to the protein binding or could it be that the anomalous DNA structure alone is responsible? The Reb1p protein is encoded by an essential gene and thus certain genetic experiments are difficult. The RNA polymerase I transcription terminator contains a Reb1p binding site and it has been demonstrated that purified Reb1p is required for transcription termination in an *in vitro* system (5). Thus, for this biological activity, it is the protein that is required. Reb1p binding sites have been identified in many promoters and it has been shown that some of these sites are required for transcription activation (6,10). It is suggested that these effects are mediated by changes in chromatin structure, for a Reb1p binding site leads to exclusion of nucleosomes (14). Further studies are needed to establish whether it is the Reb1p protein itself or the anomalous DNA structure of the Reb1p binding site that causes nucleosome exclusion and affects chromatin structure.

ACKNOWLEDGEMENTS

This work was supported by American Cancer Society grant JFRA-405 to D.R.D. and National Institutes of Health grant GM39067 to D.J.S. The DNA/Peptide facility is supported by NIH grant CA42014 and the NMR facility by grants CA42014 and RR06262.

REFERENCES

1 Ju,Q.D., Morrow,B.E. and Warner,J.R. (1990) *Mol. Cell. Biol.*, **10**, 5226–5234.
2 Morrow,B.E., Ju,Q. and Warner,J.R. (1993) *Mol. Cell. Biol.*, **13**, 1173–1182.
3 Morrow,B.E., Ju,Q. and Warner,J.R. (1990) *J. Biol. Chem.*, **265**, 20778–20783.
4 Lang,W.H. and Reeder,R.H. (1993) *Mol. Cell. Biol.*, **13**, 649–658.
5 Lang,W.H., Morrow,B.E., Ju,Q., Warner,J.R. and Reeder,R.H. (1994) *Cell*, **7984**, 527–534.
6 Brandl,C.J. and Struhl,K. (1990) *Mol. Cell. Biol.*, **10**, 4256–4265.
7 Carmen,A.A. and Holland,M.J. (1994) *J. Biol. Chem.*, **269**, 9790–9797.
8 Chasman,D.I., Lue,N.F., Buchman,A.R., LaPointe,J.W., Lorch,Y. and Kornberg,R.D. (1990) *Genes Dev.*, **4**, 503–514.
9 Erkine,A.M., Adams,C.C., Gao,M. and Gross,D.S. (1995) *Nucleic Acids Res.*, **23**, 1822–1829.
10 Remacle,J.E. and Holmberg,S. (1992) *Mol. Cell. Biol.*, **12**, 5516–5526.
11 Scott,E.W. and Baker,H.V. (1993) *Mol. Cell. Biol.*, **13**, 543–550.
12 Schlaepfer,I.R., Mattoon,J.R. and Bajszar,G. (1994) *Yeast*, **10**, 227–229.
13 Wang,H., Nicholson,P.R. and Stillman,D.J. (1990) *Mol. Cell. Biol.*, **10**, 1743–1753.
14 Fedor,M.J., Lue,N.F. and Kornberg,R.D. (1988) *J. Mol. Biol.*, **204**, 109–127.
15 Radha,P.K., Madan,A., Nibedita,R. and Hosur,R.V. (1995) *Biochemistry*, **34**, 5913–5922.
16 Lin,C.H., Hill,G.C. and Hurley,L.H. (1992) *Chem. Res. Toxicol.*, **5**, 167–182.
17 Kintanar,A., Klevit,R.E. and Reid,B.R. (1987) *Nucleic Acids Res.*, **15**, 5845–5862.
18 Marion,D., Ikura,M., Tschudin,R. and Bax,A. (1989) *J. Magn. Resonance*, **85**, 393–399.
19 States,D.J., Haberkorn,R.A. and Ruben,D.J. (1982) *J. Magn. Resonance*, **48**, 286–292.
20 Otting,G., Widmer,H., Wagner,G. and Wuthrich,K. (1985) *J. Magn. Resonance*, **66**, 187–193.
21 Rance,M., Bodenhausen,G., Wagner,G., Wuthrich,K. and Ernst,R.R. (1985) *J. Magn. Resonance*, **62**, 497–510.
22 Griesinger,C., Otting,G., Wuthrich,K. and Ernst,R.R. (1988) *J. Am. Chem. Soc.*, **110**, 7870–7872.
23 Bax,A. and Davis,D.G. (1986) *J. Magn. Resonance*, **65**, 355–360.
24 Davis,D.R. (1991) *J. Magn. Resonance*, **94**, 401–404.
25 Kessler,H., Gemmecker,G. and Steuernagel,S. (1988) *Angew. Chem. Int. Edn Engl.*, **27**, 564.
26 Kessler,H., Griesinger,C., Kerssebaum,R., Wagner,K. and Ernst,R.R. (1987) *J. Am. Chem. Soc.*, **109**, 607–609.
27 Bax,A. and Davis,D.G. (1985) *J. Magn. Resonance*, **63**, 207–213.
28 Mueller,L. (1987) *J. Magn. Resonance*, **72**, 191–196.
29 Reid,B.R., Banks,K.M., Flynn,P.F. and Nerdal,W. (1989) *Biochemistry*, **28**, 10001–10007.
30 Crippen,G.M. (1981) *Distance Geometry and Conformational Calculations.* Research Studies Press, Chichester, UK.
31 Havel,T. and Wuthrich,K. (1984) *Bull. Math. Biol.*, **46**, 673–698.
32 Hare,D.R. and Reid,B.R. (1986) *Biochemistry*, **25**, 5341–5350.
33 Hare,D.R., Shapiro,L. and Patel,D.J. (1986) *Biochemistry*, **25**, 7445–7456.
34 Banks,K.M., Hare,D.R. and Reid,B.R. (1989) *Biochemistry*, **28**, 6996–7010.
35 Feigon,J., Wright,J.M., Leupin,W., Denny,W.A. and Kearns,D.R. (1982) *J. Am. Chem. Soc.*, **104**, 5540–5541.
36 Hare,D.R., Wemmer,D.E., Chou,S.H., Drobny,G. and Reid,B.R. (1983) *J. Mol. Biol.*, **171**, 319–336.
37 Reid,B.R. (1987) *Q. Rev. Biophys.*, **20**, 1–34.
38 Kim,S.-G., Lin,L.-J. and Reid,B.R. (1992) *Biochemistry*, **31**, 3564–3574.
39 Liaw,P.C. and Brandl,C.J. (1994) *Yeast*, **10**, 771–787.
40 Kennedy,M.A., Nuutero,S.T., Davis,J.T., Drobny,G.P. and Reid,B.R. (1993) *Biochemistry*, **32**, 8022–8035.